A Comparison of Equine Infectious Anemia Virus, Human Immunodeficiency Virus Type 1, and Rous Sarcoma Virus Plasma Membrane Binding Requirements for Retrovirus Assembly

Honors Thesis
Presented to the College of Arts and Sciences,
Cornell University
in Partial Fulfillment of the Requirements for the
Biological Sciences Honors Program

by
Steven Tiwen Chen
May 2013

Supervisor: Volker Vogt

ABSTRACT

Plasma membrane (PM) association is an essential step in the retroviral life cycle that involves the complex association of the Gag polyprotein with cellular machinery, RNA, and specific lipid signatures of the inner leaflet. Here, I describe the first systematic comparison of Equine Infectious Anemia Virus (EIAV), Human Immunodeficiency Virus Type 1 (HIV-1), and Rous Sarcoma Virus (RSV) Gag membrane binding properties using *in vitro* liposome binding assays, *in vivo* virus release assays, and localization studies using confocal microscopy of 293T cells. By doing so, I hoped to address two main questions. First, what drives EIAV Gag association with the plasma membrane? And second, why is EIAV Gag not myristoylated? My results showed that EIAV Gag membrane association is driven by electrostatic interactions and a preference for cholesterol-containing membranes. These results highlight the universal importance of electrostatic interactions for retroviral Gag PM targeting and may underline a shared association with lipid raft microdomains for budding. I also used EIAV matrix (MA) and HIV-1 MA mutants to confirm HIV-1's dependence on myristoylation for virus release and localization to the plasma membrane. These same mutants have also led me to propose a model for EIAV MA helix 1 inhibition of myristoylation. Finally, a part of my thesis work has been dedicated to the development of a novel silica-bead binding assay to study protein-lipid interactions. I describe this work in Appendix 1.

INTRODUCTION

The multidomain polyprotein Gag is the main structural protein that organizes essential interactions with RNA, lipids, host cellular machinery, and itself for the assembly and budding of new retrovirus particles. The Gag protein contains three major domains: matrix (MA), capsid (CA), and nucleocapsid (NC). The MA domain controls Gag localization to the plasma membrane (PM); the CA domain mediates Gag-Gag interactions and the formation of immature virus particles; the NC domain coordinates viral genomic RNA packaging.

The big picture goal of my work was to further our understanding of the lipid signatures that drive Gag's recognition of and localization to the inner leaflet of the PM. Two phospholipid species of particular importance to retrovirus assembly are phosphatidylserine (PS) and phosphatidylinositol phosphates (PIPs). PS—which constitutes around 25-35% of inner leaflet phospholipids—has a single -1 charge that contributes to a large portion of the overall, asymmetric acidity of the PM, and is therefore important in directing the localization of proteins with polybasic regions, such as Gag (1, 2, 3, 4). PIPs have multiple negative charges that depend on specific regulation by kinases and phosphatases in different cellular compartments (5, 6). This variable distribution of PIPs in membrane compartments has been shown to be important for retrovirus trafficking (7,8), and like PS, for the localization of Gag to the plasma membrane (3, 9, 10, 11, 12, 13).

The primary interaction of Gag with membranes is through its membrane-binding domain (MBD) at the N-terminus of MA. Though retrovirus MBD sequences have largely diverged from each other, previous studies have shown MBD structural

homology and conserved basic surface patches that underline the universal importance of electrostatic interactions for Gag localization to the PM (4, 14, 15). It has also been suggested that retroviruses, such as Human Immunodeficiency Virus Type 1 (HIV-1) and Rous Sarcoma Virus (RSV), bud through lipid rafts, lipid microdomains with high liquid order phases that are enriched in unsaturated lipids, cholesterol and sphingomyelin (SM) (16, 17). Recent scholarship has also highlighted Gag's preferential targeting to unsaturated lipids, as well as its ability to distinguish acyl chain saturation and increased cholesterol concentration (18).

I began to investigate the importance of these different lipid criteria for retrovirus assembly and budding by comparing the Gag-membrane binding properties of HIV-1, RSV, and with a particular focus on Equine Infectious Anemia Virus (EIAV). Due to its relevance on human health, the majority of retroviral Gag-membrane interactions has been studied with HIV-1, which is, the best understood of these three viruses. HIV-1 membrane binding is governed by three features: a basic surface patch, a specific binding pocket for $PI(4,5)P_2$, and a 14-carbon fatty acid chain myristate group that is attached to a Glycine residue at the N-terminus of MA (3, 8, 9, 10, 11, 12, 13, 15). In vitro liposome flotation assays have shown that HIV-1 Gag binding is contingent upon, and greatly enhanced by an acidic lipid environment (3, 15, 18). Indeed, mutations in this basic surface patch cause mislocalization of Gag and a decrease in virus like particle (VLP) production (19, 20). Similarly, phosphatase-mediated depletion of $PI(4,5)P_2$ in vivo decreases both HIV-1 Gag localization to the PM and VLP production (3).

N-terminal myristoylation is the co-translational or post-translational addition of a myristate group to Glycine residues at the second position after removal of the initiating Met by N-myristoyltransferase (NMT) (21, 22, 23, 24). Though myristoylation comprises only ~1% of all fatty acids in cells, its length and saturation is uniquely capable of allowing proteins to reversibly interact with membranes (23, 24). Additional fatty acid modifications such as palmitoylation, or electrostatic interactions are needed for stable fixing to membranes (23, 24). Thus, HIV-1 Gag relies on electrostatic interactions and specific binding to $PI(4,5)P_2$ to position and secure the N-terminal myristate group into a favorable position for insertion into the lipid bilayer, thereby anchoring HIV-1 MA in the PM (13, 20, 23, 24).

Unlike HIV-1, however, RSV lacks both a myristate group and a specific $PI(4,5)P_2$ binding pocket. Though the addition of $PI(4,5)P_2$ or other PIP species enhances membrane binding in vitro, RSV MA appears to rely solely on electrostatic interactions between its basic surface patch and acidic lipid head groups for targeting to the PM (3, 14); depletion of $PI(4,5)P_2$ does not cause RSV Gag mislocalization, nor does it cause a significant decrease in VLP release (3).

Of these three retroviruses, EIAV biology and its membrane binding requirements are the least well understood. As with other retroviruses, EIAV begins its life cycle by binding to a cellular receptor (the identity of which has yet to be discovered) on horse macrophage cells with its envelope glycoprotein gp90 (25). Attachment to the cell leads to membrane fusion, and release of the EIAV capsid into the cytoplasm where the viral RNA is reverse transcribed into DNA, imported into

the nucleus, and integrated into the genome by the viral integrase (25). Rev-mediated nuclear export of transcripts allows for the translation of viral proteins in the cytoplasm that then target the plasma membrane for the assembly of new virus particles (25). Though the genomic organization of EIAV is very similar to that of its lentivirus relatives, EIAV infection in vivo displays a unique immunological phenotype. While lentiviruses such as HIV-1 are characterized by lifelong, degenerative disease, EIAV infected equids are able to transition from a chronic stage of cyclical disease to an asymptomatic state, wherein the animals no longer display disease symptoms, but are still able to transmit EIAV to non-infected animals (25, 26, 27). As a result, there is increasing interest in the potential of using EIAV as a potential model system in understanding vaccine designs for other lentiviral infections (25, 26, 27).

Like RSV Gag, EIAV Gag has been reported to not be myristoylated despite having a Glycine residue at the second position (28,29). A crystal structure of EIAV MA from 2002 showed that despite limited sequence similarity, EIAV MA likewise contains a basic surface patch and remarkable structural homology to both HIV-1 and Simian Immunodeficiency Virus (SIV) MAs (30), The current model for EIAV MA binding, based on EIAV MA crystal structure (30), and previous EIAV MA-lipid fluorescence anisotropy measurements (31), have suggested that EIAV MA interacts with the inner leaflet through electrostatic interactions and the insertion of a mobile helical hinge that partitions into the membrane head group region. This model also suggests that EIAV MA can interact with the PM with both a basic surface patch and

can roll over on the membrane surface to expose a hydrophobic face that interacts with neutral membranes (31).

Therefore, for my honors thesis, I hoped to address two main questions about EIAV Gag membrane binding. First, what drives EIAV Gag to associate with the plasma membrane? Is EIAV, like RSV, driven to the PM by electrostatic interactions? And if so, is the model put forth by Provitera et al. and others correct? That is, can EIAV Gag also interact with electrically neutral membranes? To investigate these questions, I conducted a systematic comparison of EIAV Gag binding with HIV-1 and RSV Gag binding to five different lipid compositions in an in vitro liposome-binding assay with ^{35}S radiolabeled proteins.

Second, why is EIAV Gag not myristoylated? If myristoylation does in fact enhance membrane binding and VLP production, as in HIV-1 (12, 32), why has EIAV evolved to exclude the addition of this moiety at its N-terminus? To address these questions, I made a series of point mutations at key residues in EIAV MA, along with corresponding mutations in HIV-1 MA, that have been shown to inhibit or restore myristoylation in other proteins. I investigated the effects of these mutations on myristoylation in an in vitro rabbit reticulocyte expression system in the presence of radiolabeled ^{3}H-myristic acid. I also used in vitro liposome binding assays to assess the effects of these mutations on Gag-membrane binding. Finally, I measured VLP production in transfected 293T cells by western blot and used confocal imaging of Gag-GFP to look at changes in distribution due to these mutations.

A part of my thesis research was dedicated to the development of a novel silica bead binding assay to test protein-lipid interactions. I discuss my work on this project in Appendix I.

MATERIALS AND METHODS

DNA constructs

A pPRE/EIAV Gag expression vector was generously provided by Eric Freed (NIH) for this study. I PCR amplified EIAV WT Gag sequence out of pPRE/EIAV and cloned it into pET3xc using EcoRI (nucleotide [nt]4100) and XbaI (nt6045) cut sites for T7-driven TNT reticulocyte lysate system (Promega) expression. All subsequent EIAV Gag mutants for use in this system were created using PCR-site directed mutagenesis from this initial construct. HIV-1 GagΔp6 (BH-10), HIV-1 GagΔp6 G2A(BH-10), and RSV GagΔPR were provided by Rob Dick (Cornell University). pET3xc-HIV A3D Gag was constructed using PCR-site directed mutagenesis using NdeI (nt4088) and KpnI (nt5441) cut sites.

EIAV and HIV-1 cell culture constructs were made by PCR amplifying the corresponding sequences out of their respective pET3xc plasmids into a pEGFP-N1 vector (Clontech) using EcoRI (nt629) and BamHI (nt2201) cut sites. pEGFP-N1-HIV Gag (BH10) was provided by Rob Dick (Cornell University) while pEGFP-N1-HIV Gag G2A (BH10) was provided by Marc Johnson (Cornell University). A full list of constructs and primers used in this study can be found in Supplementary Table 1.

Liposome Preparation

Liposomes were prepared using rapid solvent exchange as described (18, 33). Chloroform solutions of purified 1-Palmitoyl-2-oleoyl-sn-glycero-3-phosphocholine [POPC], 1-Palmitoyl-2-oleoyl-sn-glycero-3-phospho-L-serine [POPS], cholesterol [Chol], and L-α-phosphatidylinositol-4,5-bisphosphate [brain $PI(4,5)P_2$] were mixed to make five lipid solutions: 100%POPC, 70%POPC: 30%POPS, 34%POPC: 30%POPS:36% Chol, and 68%POPC: 30%POPS: 2%$PI(4,5)P_2$. 20 mM HEPES, pH 7.0 buffer was added to the lipid solutions in glass tubes, vortexed under vacuum for 90 seconds, and sealed under Argon gas to yield large unilamellear vesicle (LUV) solutions at 10 mg/mL. Hydrated liposomes were extruded in a mini-extruder block (Avanti) for no less than 60 times through 100-nm-polycarbonate filters (Avanti) to homogenize liposome species. All liposomes were stored at 4°C and used within 2 weeks.

Reticulocyte Expression Tests and Liposome Binding Assay

Radioactively labeled proteins were made in TNT coupled T7 rabbit reticulocyte reactions (Promega) in the presence of [^{35}S] Metionine/Cysteine (Perkin-Elmer; ExPRE35S35 protein labeling mix), Myristic Acid [9,10-^{3}H(N)]-(tetradecanoic acid) (Perkin-Elmer), or both. Reticulocyte reactions were incubated for 90 min at 30°C. Reticulocyte expression tests were carried out in 12.5 μL or 25 μL formats and run on SDS-PAGE. Gels were incubated for 30 min in 1 M sodium salicylate, dried, and developed on film at -80°C for 3-6 h (^{35}S) or up to 2 weeks (^{3}H-myr).

Liposome binding assays were conducted as previously described (3, 18). 5 μL of each reticulocyte reaction was incubated with 15 μL binding buffer (20 mM HEPES, pH 7.0) and 50 μg of LUVs at room temperature for 10 min. 80 μL of a 67% wt/wt sucrose (20 mM HEPES, pH 7.0) solution was then mixed with each binding reaction. 80 μL of this mix was then placed in a TLA-100 ultracentrifuge tube (Beckman), and layered with 120 μL 40% wt/wt sucrose (20 mM HEPES, pH 7.0), and 40 μL 4% wt/wt sucrose (20 mM HEPES, pH 7.0) solutions. Binding mixtures were centrifuged at 90,000 rpm in a TLA-100 rotor (Beckman) for 1 h. Four 60-μL fractions were collected from each reaction and resolved by SDS-PAGE. Gels were then incubated for 30 min in 1 M sodium salicylate, dried, and developed on film at -80°C for 16-48 h. The resulting autoradiograms were scanned and analyzed using ImageQuant software. The first two fractions represented liposome-bound Gag while the bottom two fractions represented non-liposome bound Gag. No less than three independent experiments were conducted for each construct and lipid type. Results were averaged and graphed using Prism 5(GraphPad Software Inc.). Error bars represent standard deviations from the mean.

Cells and Transfection

293T cells were cultured and maintained in Dulbecco's Modified Eagle Medium supplemented with 5% Fetal Bovine Serum, 5% NuSerum (BD Biosciences), and standard vitamins. 293T cells were seeded onto glass coverslips for confocal imaging or six-well plates for virus release assays 24 h prior to transfection. Cells

were transfected at 50% confluence with 2 μg DNA with FuGENE HD (Roche) per manufacturer's instructions.

Virus release and Western Blotting

To conduct virus release measurements, medium and cells were collected 24h post-transfection. The medium was centrifuged for 5 min at 5,000 x g to remove any cellular debris. Cells were collected by re-suspension in 300 μL of 1xSDS loading buffer. The collected media was then underlaid with 0.50 mL of virus suspension buffer (15% sucrose in 20 mM Tris-HCl [pH 7.5], 100 mM NaCl, 10 mM EDTA) to isolate virus-like particles (VLPs). The mixtures were then centrifuged at 90,000 rpm for 30 min in a TLA 110 rotor (Beckman). Resulting pellets were resuspended in 100 μL of 1x SDS loading buffer.

Samples were run on SDS-PAGE and transferred to a nitrocellulose membrane. Primary antibody rabbit anti-GFP, N-term (Sigma) diluted 1:2,000 followed by secondary anti-rabbit IgG-Horseradish Peroxidase (Amersham Pharmacia Biotech UK Limited) diluted 1:10,000. ChemiGlow reagent (Alpha Innotech) was added and blots were visualized by film. EIAV and HIV Gag bands were analyzed and quantified by ImageQuant software. Results were averaged and graphed using Prism 5(GraphPad Software Inc.). Error bars represent standard deviations from the mean. Statistical Significance was calculated using an unpaired student's t-test with $p<0.05$.

Confocal Microscopy

293T cells were collected 24 h after transfection and fixed with 3.7% formaldehyde in PBS for 15 min. Cells were mounted on glass slides with Fluoro-Gel (Electron-Microscopy Sciences) for imaging by Ultraview-spinning disc confocal microscope (Perkin-Elmer) with a Nikon 100x Plan-Apochromat oil objective lens (numerical aperture[NA] 1.4). Images were analyzed and generated with ImageJ software.

RESULTS

HIV-1, RSV, and EIAV Gag bind similarly to Liposomes containing POPS and Cholesterol

To understand the lipid signatures that drive EIAV Gag to the PM, I conducted a series of liposome flotation reactions and compared EIAV Gag binding with HIV-1 and RSV Gag binding. Example autoradiograms of flotations can be seen in Fig. 1A. EIAV Gag binding to 70%POPC:30%POPS liposomes was ~26%; binding increased to ~36% against 34%POPC:30%POPS:36%Chol liposomes (Fig. 1B). Similar trends were seen with HIV-1 and RSV Gag and were in accordance to results reported from previous studies (Fig. 1A-B) (3,18). Addition of 36% Cholesterol enhanced binding of EIAV Gag to 36%% therefore suggesting that like HIV-1 and RSV, EIAV Gag prefers regions of the plasma membrane with higher cholesterol concentrations (18). This also indicates that EIAV may associate with lipid raft microdomains, as inferred for HIV-1 (16, 17, 18, 34, 35) and RSV (14, 35, 36).

EIAV MA N-terminal mutations show no effect on membrane binding

N-myristoylation is the addition of a 14C saturated fatty acid chain to Glycine residues at the N-terminus of proteins by NMT (21, 22, 23, 24). The consensus sequence for N-myristoylation is generally considered to be Met-Gly-X-X-X-Ser/Thr-X-X (21, 22). Yet, despite having the necessary Glycine at the N-terminus, and a Thr at residue 5, EIAV is widely accepted to not be myristoylated (28, 29). In accordance with a study by Utsumi et al (21), I hypothesized that residues at the 3rd and 4th position of EIAV MA may inhibit myristoylation. To test this hypothesis, I constructed four EIAV Gag mutations, as well as corresponding mutations in HIV-1 (Fig. 2A), and measured the effects of these mutations on EIAV Gag (Fig. 2B) and HIV-1 Gag (Fig. 2C) binding to liposomes. I predicted that the addition of myristoylation would increase the hydrophobicity of Gag and therefore increase membrane binding.

The first mutant was an EIAV G2A mutation (Fig. 2A). If EIAV is indeed not myristoylated, this mutation should not have any effect on membrane binding. The corresponding mutation in HIV-1 however, should knock out myristoylation and therefore decrease membrane binding. My results showed that against 70%POPC: 30%POPS liposomes, EIAV G2A binding decreased from ~26% to ~21%, and from ~36% to ~24% against 34%POPC: 30%POPS: 36%Chol liposome binding when compared to EIAV WT (Fig. 2B). As expected (37, 38, 39), I saw a drop by 15% in HIV-1 G2A Gag binding against 70%POPC: 30%POPS liposomes and a drop by 30% in membrane binding with 34%POPC: 30%POPS: 36%Chol liposomes (Fig. 2C).

The second set of mutations was an EIAV D3A Gag mutation and the converse mutation HIV-1 A3D Gag, (Fig. 2A). It has been shown that Asp at the 3rd position

can inhibit myristoylation by causing a shift to N-acetylation (21). I therefore hypothesized that the EIAV D3A Gag mutation would be myristoylated, while the corresponding HIV-1 A3D mutation would inhibit N-myristoylation. While EIAV D3A Gag only showed a very small decrease in binding to 70%POPC: 30%POPS (~2%), and 34%POPC: 30%POPS: 36%Chol (~5%) (Fig. 2B), HIV-1 A3D binding decreased by ~5% to 70%POPC: 30%POPS liposomes, and by ~20% to 34%POPC: 30%POPS: 36%Chol liposomes (Fig. 2C).

The third mutant I cloned was EIAV P4A Gag (Fig. 2A). Utsumi et al. found that amino acids with radii of gyration over 1.80 A, such as Proline, could inhibit N-myristoylation (21). This phenomenon has also been shown independently in plants (40). I hypothesized that the presence of the Pro in EIAV at position 4 may play a similar inhibitory role N-myristoylation. However, again I saw comparable membrane binding with EIAV WT Gag: EIAV P4A Gag bound at ~25% to 70%POPC: 30%POPS liposomes, and at ~35% to 34%POPC: 30%POPS: 36%Chol liposomes (Fig. 2B).

Finally, I cloned an EIAV D3A P4R Gag double mutant (Fig. 2A). This mutation replaces the first four amino acids of EIAV MA with HIV-1 MA. I planned to use this construct to investigate whether downstream residues further in EIAV MA may be inhibiting N-myristoylation of EIAV MA. I plan to conduct liposome flotation reactions with this construct in the near future.

From these liposome flotation assays, I have found that changes in the first four amino acids of EIAV MA had no significant effect on membrane binding of EIAV Gag. Because each mutation slightly decreased EIAV Gag association with liposomes,

I inferred that these mutations did not induce myristoylation of EIAV Gag. These results also been confirmed by preliminary ^{3}H-myristic acid radiolabeling of EIAV WT Gag and mutants (data not shown). Though these mutations did not significantly affect EIAV Gag association, my results indicate that HIV-1 Gag binding is sensitive to mutations at the 2nd and 3rd residue position. HIV-1 G2A and A3D Gag mutations had a larger effect on HIV-1 Gag binding to 34%POPC: 30%POPS: 36%Chol liposomes, decreasing binding by about ~20%. These results not only confirm that G2A is indeed non-myristoylated, but also that the A3D mutation in HIV-1 MA may inhibit myristoylation.

EIAV Gag-GFP mutants have no significant effect *in vivo* on virus release

To investigate the effect of the EIAV Gag mutants *in vivo*, I re-cloned my EIAV and HIV-1 Gag liposome flotation constructs (Fig. 2A) into a pEGFP-N1 vector and transfected 293T cells. Consistent with the liposome binding assay results, I found no significant change in virus release of EIAV-Gag-GFP mutants from 293T cells. Virus release was measured by western blot comparison of VLP-associated Gag in the medium with the total Gag 24 h post-transfection. A representative Western Blot with cropped EIAV Gag-GFP and HIV Gag-GFP bands is shown in Figure 3A. EIAV G2A, EIAV D3A, and the double mutant EIAV D3A P4R Gag-GFP showed a slight decrease in virus release (~15%) while EIAV P4A Gag-GFP showed a slight ~15% increase in VLP release (Fig. 3B). However, no VLP release was seen in corresponding HIV-1 G2A Gag-GFP or HIV-1 A3D Gag-GFP mutants (Fig. 3B). While the identities of the HIV-1 bands were clear, there was some ambiguity about the

EIAV Gag-GFP bands due to cleavage products and unfamiliarity with viral banding patterns. In summary, I concluded that while my EIAV Gag mutants did not cause significant decreases in membrane binding, overall these mutations—with the exception of EIAV P4A Gag-GFP—did decrease virus release by ~15%. Interestingly, EIAV P4A Gag-GFP increased virus release by ~15%. In addition, virus release of HIV-1 was completely abolished in HIV-1 G2A and HIV A3D Gag-GFP mutants, therefore underlining HIV-1's dependence on myristoylation for virus release (39, 41).

EIAV Gag-GFP mutants do not show aberrant localization in 293T cells

To visualize the localization of EIAV Gag-GFP in vivo, I transfected 293T cells and imaged them using confocal microscopy 24h post-transfection. EIAV WT Gag-GFP localized to the plasma membrane and had puncta, showing VLP formation and release (Fig. 4A). A similar phenotype (Fig. 4B) was seen with EIAV G2A-Gag GFP and is consistent with in vitro membrane binding (Fig. 2B) and virus release measurements (Fig. 4B). In Fig. 4B, I also see EIAV association with endosomal compartments that has previously been reported by Fernandes et al. to be important for EIAV Gag processing (7).

HIV-1 Gag-GFP mutant transfections were carried out in parallel. As expected, HIV WT-GFP localized primarily to the plasma membrane and showed a punctate distribution, indicating virus assembly (Fig. 4C). HIV-Gag-A3D-GFP, however, showed an abnormal phenotype, localizing in clusters throughout the cell (Fig. 4D). Though confocal microscopy of HIV Gag-G2A-GFP has not yet been

performed, previous studies using electron microscopy have shown that myristoylation deficient HIV-1 Gag molecules undergo intracellular assembly (32, 42), forming virus particles without membranes. Two-photon laser scanning microscopy of HIV-1 GagΔMBD in DF-1 cells showed a similar distribution, therefore showing that the inhibition or decrease of membrane association causes aberrant distribution in cells (43). Furthermore, this same study showed that Gag-Gag interactions are not abolished in HIV-1 GagΔMBD mutants; this indicates that concentration dependent interactions of Gag in the cytoplasm are in fact sufficient for the intracellular assembly of virus particles (43). In summary, my fluorescence imaging studies of EIAV Gag-GFP WT and EIAV Gag-G2A-GFP have confirmed my in vitro liposome flotation and virus release analyses. HIV-1 A3D Gag-GFP also forms intracellular clusters which I have interpreted to be the indicative intracellular assembly of virus particles.

DISCUSSION

In this study, I addressed two main questions. First, what are the lipid signatures that drive EIAV Gag membrane association? With liposome flotation assay comparisons between HIV-1 and RSV, I have found that EIAV Gag membrane-association is driven by some of the same factors; in particular, EIAV Gag is sensitive to an acidic lipid environment and cholesterol containing membranes. This has two implications: first, like other retroviral Gags, EIAV Gag association with the PM seems to be primarily driven by electrostatic interactions. These results have been independently corroborated by computational models of EIAV MA (4), the published

crystal structure of EIAV MA (30), and fluorescence anisotropy liposome binding experiments with EIAV MA (31). Taken together, these results highlight the importance of the EIAV MA basic surface patch. Thus, using the *in vitro* liposome binding system, I have confirmed these previous models of EIAV MA binding by showing that full length EIAV Gag behaves similarly.

Second, my results suggest—albeit indirectly—that EIAV Gag may also bud from lipid raft microdomains. As seen with HIV-1 and RSV Gag, EIAV Gag sees an >10% increase in binding to liposomes with the addition of cholesterol, confirming Dick et al.'s conclusion that no fatty acid modification (ie myristoylation) is needed for the sensing and response to increased cholesterol concentrations (18). At the same time, Dick et al's results have highlighted the complexity of the retroviral response to cholesterol-containing membranes, suggesting that Gag is not just simply recognizing areas of higher lipid order (18). Rather, the addition of cholesterol seems to increase lipid packing, which makes more PS or $PI(4,5)P_2$ available for Gag-interactions (18). To investigate further, a more informative systematic study of EIAV Gag binding to high melting temperature (Tm) lipids such as SM, distearoyl phosphatidylcholine (DSPC) and to low melting Tm-lipids such as dioleoyl phosphatidylcholine (DOPC) would elaborate EIAV Gag's membrane binding capabilities, and whether it, like other retroviral Gags, can also sense the acyl chain environment (18).

The second main question of my thesis research was, why is EIAV Gag not N-myristoylated? Though EIAV Gag has the commonly accepted consensus sequence for myristoylation, M-G-X-X-X-S/T-X-X, (21, 22, 23, 24), it is widely accepted to lack

a myristoyl group 2 (8,29). To study this phenomenon, I used results by Utsumi et al. (21) as a basis to investigate whether Asp and Pro residues at the third and fourth position of EIAV MA inhibit myristoylation. Preliminary ^{3}H-myristic acid radiolableled expression in an in vitro rabbit reticulocyte system has confirmed previous HPLC-purification of EIAV Gag (28,29), which have reported that EIAV WT Gag is indeed, not myristoylated. This result was also confirmed by the EIAV G2A mutant which caused no significant decrease in binding to 70%POPC: 30%POPS and 34%POPC:30%POPS:36% Chol liposomes. Furthermore, I saw no decrease in membrane binding with EIAV D3A, or EIAV P4A Gag mutants. . That these mutants are not able to induce the addition of a myristoyl group suggest not only that the permissiveness of the consensus sequence of myristoylation may need to adjusted at these positions, but also that further downstream residues may be inhibiting myristoylation, and therefore, that the structure of EIAV MA may simply not be permissive to myristoylation.

However, these mutants consistently showed a slight decrease in membrane binding that was mirrored by a ~15% decrease in VLP production as measured by western blot with transfected 293T cells. Though these mutants may not be able to shift EIAV Gag myristoylation, they may in fact be important in EIAV Gag-membrane targeting. Interestingly, the EIAV P4A Gag mutant, which showed the least decrease in membrane binding, resulted in an increase in VLP production by 15% when compared to EIAV WT Gag. What complicates this phenomenon even further is that the EIAV D3A P4R double mutant did not exhibit the same increase in VLP production.

Though the explanation for this phenomenon remains opaque, I offer the following hypothesis. Sequence alignment of EIAV MA with HIV-1 MA by Hatanaka et al. showed that helix 1 (H1) of EIAV MA begins with a Thr-6, and continues until Val-18. The same helix in HIV-1 begins with a Leu-8 and ends with an Ile-19. Based on the crystal structure of EIAV MA and computational modeling, Hatanaka et al. have suggested that the amphipathic H1 in EIAV MA may insert itself into the head group region of the lipid bilayer, therefore serving as a protein-mediated replacement for the myristoyl anchor in HIV-1 (30). Because a Ser or Thr residue is absolutely necessary for N-myristoylation (21), I hypothesize that the participation of EIAV MA's Thr-6 in a helical structure may in fact mask NMT from recognizing the presence of this important residue. Furthermore, I posit that the P4A mutation may permit the extension of H1 to residue 4. While this may not enhance transient membrane binding to liposomes, I predict that such a mutation and extension of H1 may anchor EIAV Gag more securely once it is present at the membrane. Therefore, I believe that the model put forth by Hatanaka et al. is correct (30). According to this model, EIAV Gag, like RSV Gag, is driven to the PM by the electrostatic attractions between its basic surface patch and the acidic lipid environment of the inner leaflet. Once near the membrane, amphipathic H1 inserts into the PM, securing EIAV MA into the membrane. This model is similar to the "myristoyl-switch" model for HIV-1 Gag binding. Under this model, HIV-1 is driven in part to the PM by electrostatic interactions; specific binding to $PI(4,5)P_2$ acts as an allosteric trigger that causes a change in MA conformation (13, 41). This shift in MA conformation exposes the N-terminal myristate for insertion into the PM (13, 41). Thus, my EIAV P4A mutant

may be extending a similar insertion into the membrane by elongating H1 and therefore causing a small increase in the stable anchoring of EIAV MA. Such an interaction may enhance EIAV Gag's targeting to membrane rafts, or enhance concentration-dependent accumulation of EIAV Gag to the PM for VLP assembly and release (41, 43). Since no corresponding increase in VLP production was seen in the EIAV D3A P4R double mutant, the replacement of Pro with Arg may disrupt H1's amphipathicity and therefore, is not a permissive residue for H1 incorporation.

Interestingly, I found that the HIV-1 A3D mutation did cause a decrease in both in vitro liposome binding and an abolishment of virus release from 293T cells. This is the first time that such a mutation has been made in HIV-1 MA and has showed a dramatic effect on HIV-1 assembly. Such a phenomenon has two implications. First, the addition of an Asp residue at residue 3 can in fact inhibit myristoylation (21). Second, the myristoylation of HIV-1 Gag is necessary for VLP release. This is confirmed not only by my own HIV-1 G2A Gag results, but also in previous studies which showed that the knockout of myristoylation abolishes VLP release and leads to aberrant intracellular VLP formation in the cytoplasm (32). Therefore, the HIV A3D mutant shows that though HIV-1 Gag is able to associate transiently with membranes independently of its myristate moiety, the concentration dependent accumulation of Gag or association with membrane rafts for proper assembly is contingent on the sustained anchoring of Gag at the membrane by myristate (32, 41, 44).

There are a number of avenues to explore for future work on this project. First, a continuation of membrane binding comparisons of EIAV with HIV-1 and RSV

against a liposome panel of 100%POPC, 68%POPC: 30%POPS: 2%PI(4,5)P_2, and 40%POPC:60%POPS liposomes will be important to more broadly determine EIAV Gag's plasma membrane binding requirements. Because EIAV MA has been reported to have hydrophobic binding characteristics, I predict that EIAV Gag, but not HIV-1 or RSV, to bind at low levels to electrically neutral 100%POPC liposomes (30). Second, since EIAV Gag lacks a PI(4,5)P_2 binding pocket (30), I hypothesize that while binding to 68%POPC: 30%POPS: 2%PI(4,5)P_2 may increase, this interaction is purely due to electrostatics, and therefore EIAV Gag membrane association is not dependent on PI(4,5)P_2. This work will also need to be corroborated with *in vivo* studies using previously established methods such as phosphatase treatment to isolate the effects of PIP species abolishment on EIAV virus release(3). Third, testing against 40%POPC: 60%POPS liposomes may provide further corroboration of EIAV Gag's dependence on electrostatic interactions to get to the PM. All work should also include testing of the EIAV D3A P4R Gag double mutant binding to liposomes. Fourth, virus release western blots should be repeated with EIAV and HIV-1 Gag specific antibodies. The western blots currently used in this study were subject to some ambiguity due to unfamiliarity with EIAV Gag banding patterns and cleavage products. Repeating these results with a specific EIAV antibody will clarify the identity of the bands seen and reduce the non-specific binding seen using anti-GFP antibodies. Additional cell types should also be used to confirm results and isolate cell-type specific variation. Finally, I hope to use confocal microscopy to continue to look at EIAV and HIV-1 mutant localization in 293T cells.

Additionally, I propose three long-term goals. First, to continue with ^{3}H-myristic acid radiolabeled expression tests to confirm my EIAV MA mutant hypotheses. Second, purifying EIAV MA and using the same systematic membrane binding comparison with HIV-1 MA and RSV MA to isolate EIAV MA's interactions with the PM. Third, to do reciprocallly replace HIV-1 MA's H1 with EIAV MA's H1 to test my proposed model of EIAV Gag's MA H1 role in myristoylation inhibition.

In conclusion, I have shown that EIAV Gag is dependent on electrostatics for membrane binding. EIAV Gag also prefers cholesterol-containing membranes which may underlie a preference or dependence on budding from lipid raft microdomains. I have also shown that EIAV Gag is indeed not myristoyalted and have constructed a series of EIAV and HIV-1 MA mutations that have reaffirmed HIV-1's dependence on myristoylation for PM localization and virus release. Of these, the HIV-1 A3D mutant showed a dramatic effect on HIV-1 Gag localization to the plasma membrane, and decreased virus release. Confocal microscopy of this mutant also revealed intracellular assembly of virus particles that mirror previous microscopy results with HIV-1 G2A and HIV-1 GagΔMBD. My EIAV mutants have also led me to hypothesize that EIAV Gag is not myristoylated due to the sequestering of Thr at position 6 in H1 of EIAV MA.

APPENDIX I

INTRODUCTION

Protein-lipid interactions are essential for normal cellular activities such as signal transduction and transport. However, research in this field has been limited by the development of accurate, reproducible biochemical tests that replicate relevant physiological constraints (45). Current methods include surface Plasmon Resonance (SPR), spectroscopic methods such as fluorescence or Nuclear Magnetic Resonance (NMR), microscopy, and in vitro liposome flotation assays (45, 46). These methods however, are often time-consuming, require the use of complex equipment, and need extensive training for data interpretation. Hence, a part of my thesis research was dedicated to the development of an alternative membrane-binding assay using silica beads to meet the demand for a simple, quick method to measure protein-lipid binding.

In the Vogt lab, we are concerned with protein-lipid interactions in the context of retroviral assembly. More specifically, the big picture application of this alternative assay was to develop a more efficient way to study the lipid signatures that drive Gag's recognition, localization, and accumulation at the plasma membrane. Traditionally, these studies have primarily been performed with liposome flotation assays (3, 14, 15, 18). Liposomes with the lipid compositions of interest are incubated with protein, layered in a sucrose gradient, and spun at high speed to separate membrane bound and non-membrane fractions. The fractions are then run on SDS-PAGE, and analyzed by Coomassie staining or autoradiogram.

My proposed membrane-binding assay uses high performance liquid chromatography (HPLC) silica beads (diameter=3 μm) which are coated with C_{18} hydrocarbon chains that seed the formation of a lipid monolayer. This assay is much simpler and less time consuming than the standard liposome flotation assays used by the Vogt Lab; testing simply requires the incubation of lipid-coated beads with protein and micro-centrifugation at 5,000 rpm for 60 s to pellet the beads. No sucrose gradient is needed to separate membrane bound from non-membrane bound protein. Membrane bound protein pellets with beads during centrifugation; non-membrane protein remains in the supernatant. After SDS-PAGE, the amount of lipid-associated protein is then calculated as a ratio of pelleted, bead-associated protein to total protein loaded.

Previous studies have utilized these silica beads in a variety of ways to study protein-lipid interactions. In 2008, Yeung et al. described the use of a similar system to study the specificity of a PS probe—Lactahedrin C2. (Lact-C2) Yeung et al. measured the displacement of Lact-C2 upon the addition of PS-containing liposomes to show Lact-C2 specificity for PS (1). More recently, Alfadhi et al. (47) described the coating of silica beads with HIV-1 MA, incubation with fluorescently tagged liposomes, and measurement of bead-lipid fluorescence to determine HIV-MA phospholipid headgroup preferences. VanderVen et al. have also shown the utility of such a system for high-throughput small molecule discovery for compounds that disrupt phagosomal maturation (87). This method also depended on fluorescence measurements: fluorogenic lipid coated beads were overlaid onto a macrophage monolayer and analyzed by a fluorescent plate reader (48). What makes my

proposed system unique, however, is that it measures direct interaction of the protein with the lipid monolayer of the bead itself. While this technique can be used with fluorescent proteins as well, this alternative bead-binding assay is also amenable for analysis by SDS-PAGE for proteins without fluorescent tags.

To determine the potential of this assay for future studies of protein-lipid interactions, I purified eGFP-LactC2, the specific PS sensor advertised by Yeung et al (1, 49), and compared binding to 100% phosphatdiylcholine (PC) and 10%PS lipid coated beads with liposomes of the same compositions. I hoped to demonstrate comparable membrane-binding results to currently used technology to illustrate the usefulness of such an assay. I also investigated the effects of electrostatics and bead-surface blockers on protein-binding to the beads.

MATERIALS AND METHODS

Protein Purification

ppSUMO-eGFP-LactC2 was generously provided by Rob Dick (Cornell University) for this study. This construct was transformed into BL21 DE3/pLysS *E.coli* cells for increased protein yield. Overnight cultures of BL21 cells were grown in Lysogeny Broth (LB) with kanamycin at 37°C. Overnight cultures were diluted 1:100 in fresh medium and grown at 37°C to an optical density of 0.5 at 600 nm. Cultures were then induced with 0.5 mM isopropyl-β-D-thiogalactopyranoside (IPTG) and grown for four hours at 30°C. Cultures were pelleted and frozen at -20°C.

The frozen cell pellet were resuspended in lysis buffer (20 mM Tris-HCl, 500 mM NaCl, 1 mM phenylmethanesulfonylfluoride (PMSF). Cells were lysed by sonication and centrifuged at 90,000 rpm in a TLA-110 rotor (Beckman) at 4°C for 1h. 1 mL of supernatant was aliquoted and flash frozen for cell-extract surface blocking experiments. The rest of the supernatant was loaded onto a nickel affinity chromatography column (QIAGEN) and incubated for 2h at 4°C. The column was washed four times with 5 mL of wash buffer (20 mL of 20 mM Tris-HCl, 500 mM NaCl, 20 mM imidazole) before eluting with 10 mL of elution buffer (20 mM Tris-HCl, 500 mM NaCl, 200 mM imidazole). Fractions were analyzed by SDS-PAGE; SUMO-eGFP-LactC2 containing fractions were dialyzed overnight at 4°C in Dialysis buffer (20 mM Tris-HCl, 500 mM NaCl, pH 7) and supplemented with previously purified Ubl-specific protease 1 (ULP). ULP protease is highly specific for the SUMO protein and used to cleave SUMO from eGFP-LactC2. Dialyzed fractions were loaded onto a nickel affinity chromatography column (QIAGEN) and incubated for 2h at 4°C. Column was washed twice with 5 mL of 20 mM Tris-Hcl, 500 mM NaCl, pH 7. eGFP-LactC2 was eluted twice with 5 mL of wash buffer. 5 mL of elution buffer was added to elute off ULP protease. Fractions were analyzed by Coomassie-Blue stained SDS-PAGE. Protein containing fractions were concentrated to approximately 15 mg/mL with an Ambicon (Millipore) tube. Protein was flash frozen in an Ethanol-Dry Ice bath and stored at -80°C in 20% glycerol and 10 mM dithiothreitol (DTT). Protein purification gels can be seen in Appendix Fig. 1.

Preparation of lipid-coated silica beads

Silica Nucleosil C18 reverse phase HPLC beads (diameter= 3 μm) were coated with lipids as previously described (47) with modifications. 20 mg of beads were dissolved in 2 mL of chloroform and stored at 4°C. To make 100% PC beads, 0.231 mg of egg-PC (Avanti) in chloroform was added to 200 μL of beads. To make 90%PC: 10%PS beads, 0.208 mg of egg-PC and 0.025 mg brain-PS (Avanti) were added to 200 μL of beads. Approximately 100x more lipid was added than needed to ensure complete coverage of bead surfaces. Beads and lipid solution were dried down with N_2 gas. 200 μL bead preparation buffer (20 mM HEPES, 100 mM NaCl, pH 7) was added to dried beads and sonicated in a water bath while pipetting up and down to resuspend beads. Lipid coated beats were washed with 200 μL of bead preparation buffer by vortexing and centrifugation at 5,000 rpm for 1 min three times. Beads were stored in 200 μL of bead preparation buffer at a final concentration of 100 mg/mL at 4°C before use.

Silica bead binding Assay

Approximately 3 μg of eGFP-LactC2 was added to 1 mg of beads. Each protein aliquot was spun at 14,000 rpm for 10 min at 4°C to pellet any aggregated protein. Mixtures were incubated on ice for 10 minutes. Beads were washed twice with 100 μL buffer by pipetting up and down and centrifuged at 5,000 rpm for 5 min to pellet beads and protein. All buffers used were 20 mM HEPES at final NaCl concentrations of 100, 300, or 500 mM NaCl. NaCl concentrations were varied to assess the effects of electrostatics on eGFP-LactC2 binding to the lipid-coated beads. After 2nd wash, beads were resuspended in 30 μL of buffer and centrifuged at 5,000 rpm for 5 mins.

Supernatant, 30 μL from each wash, and beads were run on SDS-PAGE. Gels were analyzed after Coomassie staining by measuring dividing of protein in bead fraction by total protein loaded. All quantification was performed in ImageQuant software.

Bead surface blocking experiments were carried out with either addition of SUMO-eGFP LactC2 purification cell extract or with Bovine Serum Albumin (NEB). Cell extract aliquots were spun at 14,000 rpm for 10 min at 4°C to spin down any aggregates. 10 μL of cell extract was incubated with beads and proteins on ice for 10 mins. Similarly, 0.01 mg of BSA was added during incubation to block bead surface from non-specific binding. NaCl concentrations of buffers were altered to maintain 100, 300, or 500 mM NaCl balance.

Liposome Preparation

Liposomes were prepared using rapid solvent exchange as described (18, 33). Chloroform solutions of purified L-α-phosphatidylcholine (Egg, Chicken) [Avanti] and L-α-phosphatidylserine (Brain, Porcine) [Avanti] were mixed to make 100%PC and 90%PC: 10%PS liposomes. 20 mM HEPES, pH 7.0 buffer was added to the lipid solutions in glass tubes, vortexed under vacuum for 90 seconds, and sealed under Argon gas to yield large unilamellear vesicle (LUV) solutions at 10 mg/mL. Hydrated liposomes were extruded in a mini-extruder block (Avanti) for no less than 60 times through 100-nm-polycarbonate filters (Avanti) to homogenize liposome species. All liposomes were stored at 4°C and used within 2 weeks.

Liposome Binding Assay

Liposome binding assays were conducted as previously described (18). 5 μg of eGFP-LactC2 was incubated with 15 μL binding buffer (20 mM HEPES, pH 7.0) and 50 μg of LUVs at room temperature for 10 min. Incubation was performed at either 160 (physiological) or 300 mM NaCl. 80 μL of a 67% wt/wt sucrose (20 mM HEPES, pH 7.0) solution was then mixed with each binding reaction. 80 μL of this mix was then placed in a TLA-100 ultracentrifuge tube (Beckman), and layered with 120 μL 40% wt/wt sucrose (20 mM HEPES, pH 7.0), and 40 μL 4% wt/wt sucrose (20 mM HEPES, pH 7.0) solutions. Binding mixtures were centrifuged at 90,000 rpm in a TLA-100 rotor (Beckman) for 1 h. Four 60-μL fractions were collected from each reaction and resolved by SDS-PAGE. Gels were Coomassie stained and analyzed with ImageQuant software. The first two fractions represented liposome-bound Gag while the bottom two fractions represented non-liposome bound Gag. Results were averaged and graphed using Prism5 (GraphPad Software). Error bars represent standard deviations from the mean. No less than three independent experiments were conducted for each construct and lipid type.

RESULTS

Purification of eGFP-LactC2

Appendix Fig. 1 shows an example of an eGFP-LactC2 purification. Protein was expressed using a ppSUMO backbone in BL21-DE3/pLysS *E.coli* cells. SUMO-eGFP LactC2 can be seen at ~67 kDa in Appendix Fig. 1A. ULP protease was used to cut off SUMO tag to yield eGFP-LactC2, ~45 kDa (Appendix Fig. 1A-B). SUMO Tag (~12 kDa) and ULP Protease (~26 kDa) can be seen in Appendix Fig. 1B, lane 5.

Purified protein was concentrated using Ambicon (Millipore) filter and stored in 20% glycerol with 10 mM DTT. Protein was stored at -80°C until use.

eGFP-LactC2 binds similarly to Silica Beads and Liposomes

To assess the utility of my silica bead binding assay, I compared eGFP-LactC2 binding to both 100%PC and 90%PC:10%PS beads and liposomes. In Appendix Fig. 2A, supernatant, wash, and bead fractions were loaded onto SDS-PAGE. Consistenly, a non-significant amount of eGFP-Lactc2 was eluted from beads during washes, suggesting a stable interactions with lipids on beads. eGFP-LactC2 showed ~30% binding to 100%PC beads and ~40% binding to 90%PC:10%PS beads. Because eGFP-LactC2 has been previously reported by Yeung et al. to show no relative binding to PC beads (1), I hypothesized that binding to PC-silica beads was due to non-specific binding to uncoated silica bead surfaces. To assess whether increasing NaCl concentrations could cause eGFP-LactC2 to bind more discriminately, I conducted binding experiments with increasing NaCl concentrations (Appendix Fig. 2B-2C). Appendix Fig. 2B is a representative example of a eGFP-LactC2 binding to 100%PC and 90%PC:10%PS silica beads at 100, 300, and 500 mM NaCl. I found that while eGFP-LactC2 binding to 100%PC decreased slightly with increasing NaCl concentration, there was no significant decrease in binding to 90%PC:10%PS beads.

In Fig. 2D, I show an example of a purified eGFP-LactC2 binding experiment to 100%PC liposomes at 160 mM and 300 mM NaCl. Because eGFP-LactC2 was stored at 500 mM NaCl, 100 mM NaCl binding experiments were not performed because of volume restrictions of the liposome flotation assay. Similarly, in

Appendix Fig. 2E, I show an example of an eGFP-LactC2 binding experiment to 90%PC:10%PS liposomes at 160 and 300 mM NaCl. I found that eGFP-LactC2 showed comparable binding to silica beads at 100 mM NaCl, and to 100%PC liposomes at 160 mM NaCl (Fig. 1F). As with binding to silica beads, I saw 5% decrease in eGFP-LactC2 binding to 100%PC liposomes at 300 mM NaCl. Furthermore, I saw similar binding results, ~30% binding to 90%PC:10%PS beads at both salt concentrations.

From these results, I concluded that eGFP-LactC2 binds similarly to both silica beads and liposomes of the same compositions. Furthermore, I concluded that eGFP-LactC2 specificity is dependent on electrostatics. However, in contrast to previously reported results by Yeung et al., eGFP-LactC2 also seems to have hydrophobic binding capability to electrically neutral membranes. To corroborate my results, I conducted a series of bead-surface blocking experiments to isolate non-specific binding of eGFP-LactC2 to the silica bead from its promiscuity to binding electrically neutral membranes.

Non-specific binding of eGFP-LactC2 to silica bead surface is reduced by addition of BSA or Cell Extract

In Appendix Fig. 3, I compared the effects of eGFP-LactC2 binding to 100%PC and 90%PC:10%PS silica beads with two blocking agents: BSA and cell extract. Appendix Fig. 3A is a representative SDS-PAGE of a binding experiment with BSA. The lower band, at approximately 45 kDa is eGFP-LactC2 while the upper band, at 65 kDa is BSA. Fig. 3B is a representative SDS-PAGE of a binding experiment with

cell extract. Cell extract was prepared after sonication and centrifugation of cell pellets during eGFP-LactC2 protein purification. CE was flash frozen, and spun down at 14,000 rpm for 10 min at 4°C to spin down any aggregated protein. I hypothesized that the addition of cell extract would supplement the binding mixture with proteins that would bind to uncoated bead surfaces to block non-specific binding of eGFP-LactC2. The lower band at 45 kDa is eGFP-LactC2 while the prominent upper band at ~67 kDa is SUMO-eGFP-LactC2. With BSA, eGFP-LactC2 consistently bound at ~20% to 100%PC silica beads (Appendix Fig.3C). Furthermore, adding BSA as a surface blocker did not cause a decrease in eGFP-LactC2 binding with increasing NaCl concentrations. eGFP-LactC2 bound at similar levels to BSA-free 90%PC:10%PS silica beads, ~45% at all NaCl concentrations. Panel 3D shows quantification of eGFP-LactC2 binding with cell extract as a blocking agent. Binding was similar to BSA-blocked binding: eGFP-LactC2 bound at a consistent ~20% to 100%PC silica beads, and at ~35% to 90%PC:10%PS beads. There was no decrease in eGFP-LactC2 binding to cell-extract blocked 100%PC beads with increasing NaCl but eGFP-LactC2 binding to CE-blocked beads showed much greater heterogeneity.

Appendix Fig. 3 shows that blocking with either BSA or CE does indeed prevent some non-specific binding to the non-lipid coated bead surfaces. Because BSA blocked beads showed more consistent binding reuslts, it may be a better candidate for surface blocking than cell extract. In contrast to previously published results, I concluded that eGFP-LactC2 does indeed bind at ~20% to electrically neutral membranes. A comparison of Appendix Fig. 2 and Appendix Fig. 3 suggests

that approximately 10% of eGFP-LactC2 binding to unblocked 100%PC silica beads was due to non-specific binding to the bead surface. While electrostatics caused non-specific binding to decrease in the absence of a blocking agent, increasing salt concentrations did not cause a significant change to eGFP-LactC2 binding to 100%PC beads. Together, these results demonstrate that eGFP-LactC2 binding to electrically neutral membranes is a specific interaction and not dependent on electrostatic interactions.

DISCUSSION

I began an investigation into the potential of using lipid coated 3 μm diameter HPLC silica beads as an alternative membrane binding platform for studying protein-lipid interactions. BecauseLactC2, the C2 domain of the Lactahedrin protein, has been previously been reported by Yeung et al. to be a very specific PS sensor (1), I decided to purify eGFP-LactC2 to undergo some control binding experiments to determine the utility of this assay. In contrast to Yeung et al.'s results, I found that eGFP-LactC2 binds at ~20% to 100%PC membranes, therefore showing that eGFP-LactC2 is not nearly as specific as previously advertised (1). These results were confirmed by purified eGFP-LactC2 flotations with 100%PC liposomes and by in vitro rabbit reticulocyte translated eGFP-LactC2 flotations (Katherine Konvinse [Cornell University]- unpublished results). A crystal structure of LactC2 revealed 2 hydrophobic spikes that are predicted to insert themselves into membranes (50), which may explain eGFP-LactC2's binding to electrically neutral membranes. At the same time, I did find that eGFP-LactC2

increases by 10-20% with the addition of 10%PS; this suggests that eGFP-LactC2 is indeed senstive to PS, but that this membrane association may be contingent on, or greatly enhanced by anchoring in electrically neutral lipid environments.

Though 100x more lipid was added than needed to coat bead surfaces, I showed that binding of eGFP-LactC2 to 100%PC beads varied in the presence surface blocking agents, therefore demonstrating that some non-specific binding to the silica bead surface occurs. I used two different blocking strategies, BSA and cell extract, and showed that both strategies yielded similar membrane binding results. However, the addition of BSA results in less variation which may make it the better blocking agent for future studies. Moreover, adding surface blocking agents to binding reactions stabilized specific binding in increasing NaCl concentrations. These results show that these beads can be used to achieve stable, consistent binding at a physiological, ~160 mM NaCl, salt concentration.

Though these results are a promising start for future work on this assay, a number of problems and limitations remain. First, bead coating should be attempted with fluorescent lipid probe mixtures to evaluate coating on the bead surface. This will also determine whether irregular lipid distributions form on the bead surface that may affect protein-lipid interactions. Second, binding experiments of known proteins with known behavior should be conducted and compared with liposome flotation results. Third, more complex lipid mixtures should be coated onto bead surfaces to measure protein binding to more physiologically relevant lipid environments. This may include the addition of cholesterol, charged PIP species, or lipids of varying saturation and may increase the uses of this assay in protein

binding response to parameters such as lipid order. I have previously attempted to make beads with higher PS concentrations (>30%PS) but found that coating was less efficient, perhaps due to electrostatic repulsion. Electrostatic repulsion between beads also seemed to prevent efficient pelleting in microcentrifuge tubes. Binding with silica beads with higher PS concentrations gave varied, inconsistent results (data not shown). These results suggest coating with charged lipids may result in irregular distributions on the bead surface and therefore, different concentrations of lipid coating on the surface than expected. Furthermore, inefficient pelleting of beads may have also resulted in changes in the amount of beads present in each binding reaction. Hence, further modifications of bead preparation buffer, such as increasing ionic strength, may alleviate some of these issues.

In conclusion, I have shown that this silica bead binding assay may be a new and more efficient way to study protein-lipid interactions. My results showed that though eGFP-LactC2 is indeed sensitive to PS, it also binds to 100%PC Silica beads and 100%PC liposomes. These results, along with unpublished data by Katherine Konvinse (Cornell University), have shown that previous reports of LactC2 specificity may be incorrect. I also conducted testing on the effects of bead surface blocking agents on eGFP-LactC2 binding and found that the addition of BSA not only reduced non-specific binding, but also resulted in more consistent binding in my assay. Future testing should be conducted with different proteins of known behavior and lipid compositions to expand the utility of this assay to future protein-lipid interaction studies.

REFERENCES

1. Yeung, T et al. 2008. Membrane Phosphatidylserine Regulates Surface Charge and Protein Localization. Science. 319(5860): 210-213.

2. Leventis, PA., and Grinstein, S. 2010. The distribution and function fo phosphatidylserine in cellular membranes. Annu Rev Biophys. 39:407-27.

3. Chan, J., Dick, RA., Vogt, VM. 2011. Rous sarcoma virus gag has no specific requirement for phosphatidylinositol-(4,5)-bisphosphate for plasma membrane association in vivo or for liposome interaction in vitro. J Virol. 85(20): 10851-60.

4. Murray, PS et al. 2005. Retroviral matrix domains share electrostatic homology: models for membrane binding function throughout the viral life cycle. Structure. 13(10):1521-31.

5.Di Paolo, G., and De Camilli, P. 2006. Phosphoinositides in cell regulation and membrane dynamics. Nature. 443(7112):651-7.

6. Kutateladze, TG. 2010. Translation of the phosphoniositide code by PI effectors. Nat Chem Biol. 6(7): 507-13.

7. Fernandes, F. et al. 2011. Phosphoinositides direct equine infections anemia virus gag trafficking and release. Traffic. 12(4): 438-51.

8. Ono, A. et al. 2004. Phosphatidylinositol (4,5) bisphosphate regulates HIV-1 Gag targeting to the plasma membrane. Proc Natl Acad Sci USA. 101(41): 14889-14894.

9. Anraku, K. 2010. Highly sensitive analysis of the interaction between HIV-1 Gag and phosphoinositide derivatives based on surface Plasmon resonance. Biochemistry. 49(25): 5109-16.

10. Campbell, S. et al. 2001. Modulation of HIV-like particle assembly in vitro by inositol phosphates. Proc Natl Acad Sci USA. 98(19): 10875-10879.

11. Chan, R. et al. 2008. Retroviruses human immunodeficiency virus and murine leukemia virus are enriched in phosphoinositides. J Virol. 82(22): 11228-38.

12. Chukkapalli, V., et al. 2008. Interaction between the Human Immunodeficiency Virus Type 1 Gag Matrix Domain and Phosphatidylinositol-(4,5)- Bisphosphate is Essential for Efficient Gag Membrane Binding. J Virol. 82(5): 2405-2417.

13. Saad, JS., et al. 2006. Structural basis for targeting HIV-1 Gag proteins to the plasma membrane for virus assembly. Proc Natl Acad Sci USA. 103(30): 11364-11369.

14. Dalton, AK., Murray, PS., Murray, D., Vogt, VM. 2005. Biochemical chracterization of Rous Sarcoma Virus MA protein interaction with membranes. J Virol. 79(10): 6227-38.

15. Dalton, AK. et al. 2007. Electrostatic Interactions Drive Membrane Association of the Human Immunodeficiency Virus Type 1 Gag MA Domain. J Virol. 81(12): 6434-6445.

16. Brügger, B., et al. 2006. The HIV lipidome: a raft with an unusually composition. Proc Natl Acad Sci USA. 103(8): 2641-6.

17. Waheed, AA., and Freed, EO. 2009. Lipids and membrane microdomains in HIV-1 replication. Virus Res. 143(2): 162-76.

18. Dick, RA., Goh, SL., Feigenson, GW., Vogt, VM. 2012. HIV-1 Gag protein can sense the cholesterol and acyl chain environment in model membranes. Proc Natl Acad Sci USA. 109(46): 108761-18766.

19. Freed, EO., Orenstein, JM., Buckler-White, AJ., Martin, MA. 1994. Single amino acid changes in the Human Immunodeficiency Virus Type 1 Matrix block virus particle production. J Viro. 68*8): 5311-5320.

20. Scarlata, S., and Carter, C. 2003. Role of HIV-1 Gag domains in viral assembly. Biochim Biophys Acta. 1614(1): 62-72.

21. Utsumi, T., et al. 2001. Amino acid residue penultimate to the amino-terminal gly residue strongly affects two modifications, N-myristoylation and N-acetylation. J Biol Chem. 276(13): 10505-13.

22. Boutin, JA. 1997. Myristoylation. Cell. Signal. 9(1): 15-35.

23. Martin, DDO., Beauchamp, E., Berthiaume, LG. 2011. Post-translational myristoylation: Fat matters in cellular life and death. Bioactive Lipids, Nutrition and Health. 93(1): 18-31.

24. Maruer-Stroh, S.., Eisenhaber B., Eisenhaber, F. 2002. N-terminal N-myristoylation of proteins: refinement of the sequence motif and its taxon-specific differences. J Mol Biol. 317(4): 523-40.

25. Leroux, C., Cadoré, JL., Montelaro, RC. 2004. Equine Infections Anemia Virus (EIAV): what has HIV's country cousin got to tell us? Vet Res. 35(4): 485-512.

26. Criago, JK., et al. 2005. Discerning an effective balance between equine infections anemia virus attenuation and vaccine efficacy. J Virol. 79(5): 2666-77.

27. Craigo, JK and Montelaro, RC. 2011. Equine Infectious Anemia Virus Infection and Immunity: Lessons for AIDS Vaccine Development. Future Virol. 6(2): 139-142.

28. Henderson, LE., Sowder, RC., Smythers, GW., Oroszlan, S. 1987. Chemical and Immunoglocail Characterization of Equinte Infectious Anemia Virus gag-Encoded Proteins. J Virol. 61(4): 1116-1124.

29. Ball, JM et al. 1988. Lentivirus antigen purification and characterization: isolation of equine infectious anemia virus gag and env proteins in one step by reverse phase HPLC and application to human immunodeficiency virus glycoproteins. Journal of Virological Methods. 19: 265-277.

30. Hatanaka, H., et al. 2002. Structure of Equine Infectious Anemia Virus Matrix Protein. J Virol. 76(4): 1876-1883.

31. Provitera, P., et al. 2000. Binding of Equine Infectious Anemia Virus Matrix Protein to Membrane Bilayers Involves Multiple Interactions. J. Mol Biol. 296:887-898.

32. O'Carroll, IP., et al. 2012. Funcational Redundancy in HIV-1 viral particle assembly. J Virol. 86(23): 12991-6.

33. Buboltz, JT and Feigenson, GW. 1999. A novel strategy for the preparation of liposomes: Rapid solvent exchange. Biochim Biophys Act. 1417(2):232-45.

34. Ono, A., and Freed, EO. 2001. Plasma membrane rafts play a critical role in HIV-1 assembly and release. Proc Natl Acad USA. 98(24): 13925-13930.

35. Briggs, JAG., Wilk, T., and Fuller, SD. 2003. Do lipid rafts mediate virus assembly and pseudotyping? Journal of General Virology. 84(4): 757-768.

36. Quigley, JP., Rifkin, DB., Reich, E. 1971. Phospholipid composition of Rous sarcoma virus membranes and other enveloped RNA viruses. Virology. 46(1): 106-116.

37. Morikawa, Y., Hockley, DJ., Nermuet, MV., Jones, IM. 2000. Role of Matrix, p2, and N-terminal Myristoylation in Human Immunodeficiency Virus Type 1 Gag Assembly. J Virol. 74(1): 16-23.

38. Ghanam, RH., Samal, AB., Fernandez, TF., Saad, JS. 2012. Role of the HIV-1 Matrix Protein in Gag Intracellular Trafficking and Targeting to the Plasma Membrane for Virus Assembly. Front Microbiol. 3(55): 1-15.

39. Pal, R. et al. 1990. Myristoylation of gag proteins of HIV-1 plays an important role in virus assembly. AIDS Res Hum Retroviruses. 6(6): 721-30.

40. Yamauchi, S., et al. 2010. The consensus motif for N-myristoylation of plant proteins in a wheat germ cell-free translation system. FEBS J 277(17): 3596-607.

41. Ono, A. 2009. HIV-1 Assembly at the Plasma Membrane: Gag Trafficking and Localization. Future Virol. 4(3): 241-257.

42. Jouvenet, N., et al. 2006. Plasma Membrane is the Site of Productive HIV-1 Particle Assembly. PLoS Biology. 4(12): 2296-2310.

43. Larson, DR., Ma, YM., Vogt, VM., Webb, WW. 2003. Direct Measurement of Gag-Gag interaction during retrovirus assembly with FRET and fluorescence correlation spectroscopy. The Journal of Cell Biology. 162(7): 1233-1244.

44. Lindwasser, OW., and Resh, MD. 2002. Myristoylation as a target for inhibiting HIV assembly: Unsaturated fatty acids block viral budding. Proc Natl Acad Sci USA. 99(20): 13037-13042.

45. Heyse, S., et al. 1998. Emerging techniques for investigating molecular interactions at lipid membranes. Biochim Biophys Acta. 1376(3): 319-38.

46. Besenicar, M., Macek, P., Lakey, JH., Anderluh, G. 2006. Surface plasmon resonance in protein-membrane interactions. Chem Phys Lipids. 141(1-2): 169-78.

47. Alfadhli, A., et al. 2011. HIV-1 matrix protein bidning to RNA. J Mol Biol. 410(4): 653-66.

48. VanderVen, BC., et al. 2010. Development of a novel, cell-based chemical screen to identify inhibitors of intraphagosomal lipolysis in macrophages. Cytometry A. 77(8): 751-60.

49. Kay, JG., Grinstein, S. 2011. Sensing phosphatidylserine in cellular membranes. Sensors. 11(2): 1744-55.

50. Shao, C., et al. 2008. Crystal structure of lactahedrin C2 domain at 1.7 A resolution with mutational and computational analyses of its membrane-binding motif. J Biol Chem. 283(11): 7230-41.

ACKNOWLEDGEMENTS

This work would not have been possible wihtout Rob Dick, not only for providing pET-HIV WT, pET-RSV WT, pEGFP N1-HIV WT, but also for the invaluable mentorship and feedback throughout this whole process. I am forever grateful for your teaching and guidance. I would also like to thank Prof. Volker Vogt for his mentoring, patience, and for helping me to develop as a scientist and scholar; your genius, humility, and optimism have inspired me more than you know. I also want to thank the other Vogt Lab Members, past and present, for laying the groundwork for this work. In particular, Di Luo, Kat Konvinse, Nischay Rege, and Bosh Bhowmick for making lab a wonderful place to be. Thank you for sharing your space, time, knowledge, and friendship with me these past three years. I also acknowledge Eric Freed (NIH) for providing pPRE/EIAV Gag expression vector and Marc Johnson for pEGFP-N1 HIV G2A Gag-GFP. Finally, I would like to thank my family. To my parents: thank you for your sacrifices, and for enduring the hardships it took for me to come to Cornell. I am undeserving of your unwavering love and support. And to my brother Spencer: thank you for everything. I would not be where I am today without you.

FIGURE LEGENDS

FIG.1 Liposome binding assay comparison of EIAV Gag with HIV-1 and RSV Gag. (A) Example of HIV-1, RSV, EIAV Gag flotation autoradiograms against two liposome compositions. Top two fractions were interpreted as membrane bound (MB) while bottom two fractions were non-membrane bound (NMB). Amount of binding was calculated by dividing MB Gag by total Gag. (B) Average binding against 70%POPC:30%POPS and 34%POPC:30%POPS:36%Chol liposomes. Quantification was performed of no less than three flotation reactions for each composition. Error bars represent standard deviations from the mean.

FIG.2 Liposome binding assay comparison of EIAV and HIV-1 mutants against 70%POPC:30%POPS and 34%POPC:30%POPS:36%Chol liposomes. (A) N-terminal sequences of EIAV and HIV-1 mutants adapted with modifications from Hatanaka et al (30). Red denotes mutated amino acid residues; blue denotes conserved residues. Helix 1 (H1) is marked for each virus. (B) Quantification of EIAV mutants and (B) HIV mutants. Binding was performed with two lipid types: 70%POPC:30%POPS and 34%POPC:30%POPS:36%Chol. EIAV Gag and HIV-1 WT Gag results were included to serve as comparisons. Quantification was performed of no less than three flotation reactions for each composition. Error bars represent standard deviations from the mean.

FIG.3 EIAV Gag-GFP and HIV Gag-GFP mutant virus release from 293T cells.

(A) Example of a Western Blot cropped bands of EIAV Gag-GFP and HIV Gag-GFP. VLPs were collected from medium 24h post-transfection and compared to lysed cell fractions. Amount of Gag-GFP released was analyzed with Western blot analysis. (B) Quantification of % Virus release was calculated as the amount of extracellular Gag divided by total Gag. Error bars represent standard deviations from the mean from three independent experiments. Significance, calculated using an unpaired student t-test is shown with asterisks.

FIG. 4. EIAV and HIV Gag-GFP localization in 293T cells.
293T cells were transfected with (A) EIAV-WT Gag-GFP, (B) EIAV WT Gag G2A GFP, (C) HIV-WT Gag-GFP, and (D) HIV-WT A3D Gag-GFP. Images are representative of cells after one experiment.

Appendix FIG. 1 Example of eGFP-LactC2 Purification.
30 μL of each fraction during each purification step was loaded. eGFP-LactC2 was by using a ppSUMO expression plasmid. (A) Coomassie-Blue stained SDS-PAGE of eGFP-LactC2 purification. Lanes: (1) Ladder (Promega) (2) Post-spin: crude supernatant after sonication and centrifugation at 90,000 rpm for 1 h at 4°C. Supernatant was incubated with NI-NTA beads (QIAGEN) for 2 h at 4°C. (3) Flowthrough (FT): flowthrough fraction after running supernatant through Ni-NTA column (4-7) Washes 1-4 (W1-4). Each wash was performed with 5 mL of Wash Buffer. (8) Elution 1 (E1): 10 mL of elution buffer was used to elute SUMO-eGFP-LactC2 off column. Elution fraction was dialyzed overnight with ULP protease in 20

mM Tris, 500 mM NaCl, pH 7 overnight to dilute imidazole. Dialyzed fraction was incubated Ni-NTA beads for 2 h at 4°C. (9) Flowthrough 2(FT2): flowthrough fraction after running dialyzed supernatant through Ni-NTA column. (10) Wash (W1): wash was performed with 5 mL of 20 mM Tris, 500 mM NaCl, pH 7. (B) Continuation of eGFP-LactC2 purification: Coomassie-Blue stained SDS-PAGE of eGFP-LactC2 purification. (1) Ladder. (2) Wash (W2): wash was performed with 5 mL of dialysis buffer. (3) Elution 1 (E1): eGFP-LactC2 was eluted after incubation for 30 min at 4°C with 5 mL of Wash Buffer. (4) Elution 2 (E2) eGFP-LactC2 with 5 mL of Wash Buffer. (5) Elution 3 (E3) eGFP-LactC2 with 5 mL of Elution Buffer.

Appendix FIG.2 Comparison of eGFP-LactC2 binding to silica beads and liposomes at different NaCl concentrations.

(A) Example of Coomassie-Blue stained SDS-PAGE showing eGFP-LactC2 binding to 100%PC and 90%PC:10%PS silica beads at 100 mM NaCl. Supernatant (S), washes (W), and pelleted beads (B) are shown. (B) Example of Coomassie-Blue stained SDS-PAGE of eGFP-LactC2 binding to 100%PC and 90%PC:10%PS silica beads to a panel of 100, 300, 500 mM NaCl to assess effects of electrostatics of eGFP-LactC2 binding. (C) Quantification of eGFP-LactC2 binding to 100%PC and 90%PC:10%PS silica beads at 100, 300, 500 mM NaCl. Quantification was performed of no less than three separate binding reactions for each composition. Error bars represent standard deviations from the mean. (D) Coomassie-Blue stained SDS-PAGE of purified eGFP-LactC2 binding to 100%PC liposomes at 160 and 300 mM NaCl. Top two fractions represent membrane bound; bottom two fractions represent non membrane bound

fraction. (e) As in D, except with 90%PC:10%PS liposomes. (F) Quantification of eGFP-LactC2 binding to 100%PC and 90%PC:10%PS liposomes at 160 and 300 mM NaCl. Quantification was performed of no less than three separate flotation reactions for each composition. Error bars represent standard deviations from the mean.

Appendix FIG. 3 Silica bead binding experiments with surface blockers BSA or cell extract (CE).

(A) Example of SDS-PAGE of eGFP-LactC2 binding to 100%PC and 90%PC:10%PS silica beads with BSA as blocking agent. Binding was performed to panel of 100, 300, 500 mMNaCl. (B) Example of SDS-PAGE of eGFP-LactC2 binding to 100%PC and 90%PC:10%PS silica beads with CE as blocking agent. Binding was performed to panel of 100, 300, 500 mMNaCl. (C) Quantification of eGFP-LactC2 binding to 100%PC and 90%PC:10%PS silica beads with BSA at 100, 300, 500 mM NaCl. Quantification was performed of no less than three separate binding reactions for each composition. Error bars represent standard deviations from the mean. (D) Quantification of eGFP-LactC2 binding to 100%PC and 90%PC:10%PS silica beads with CE at 100, 300, 500 mM NaCl. Quantification was performed of no less than three separate binding reactions for each composition. Error bars represent standard deviations from the mean.

Supplementary Table 1 List of constructs and primers used in this study.

Fig. 1

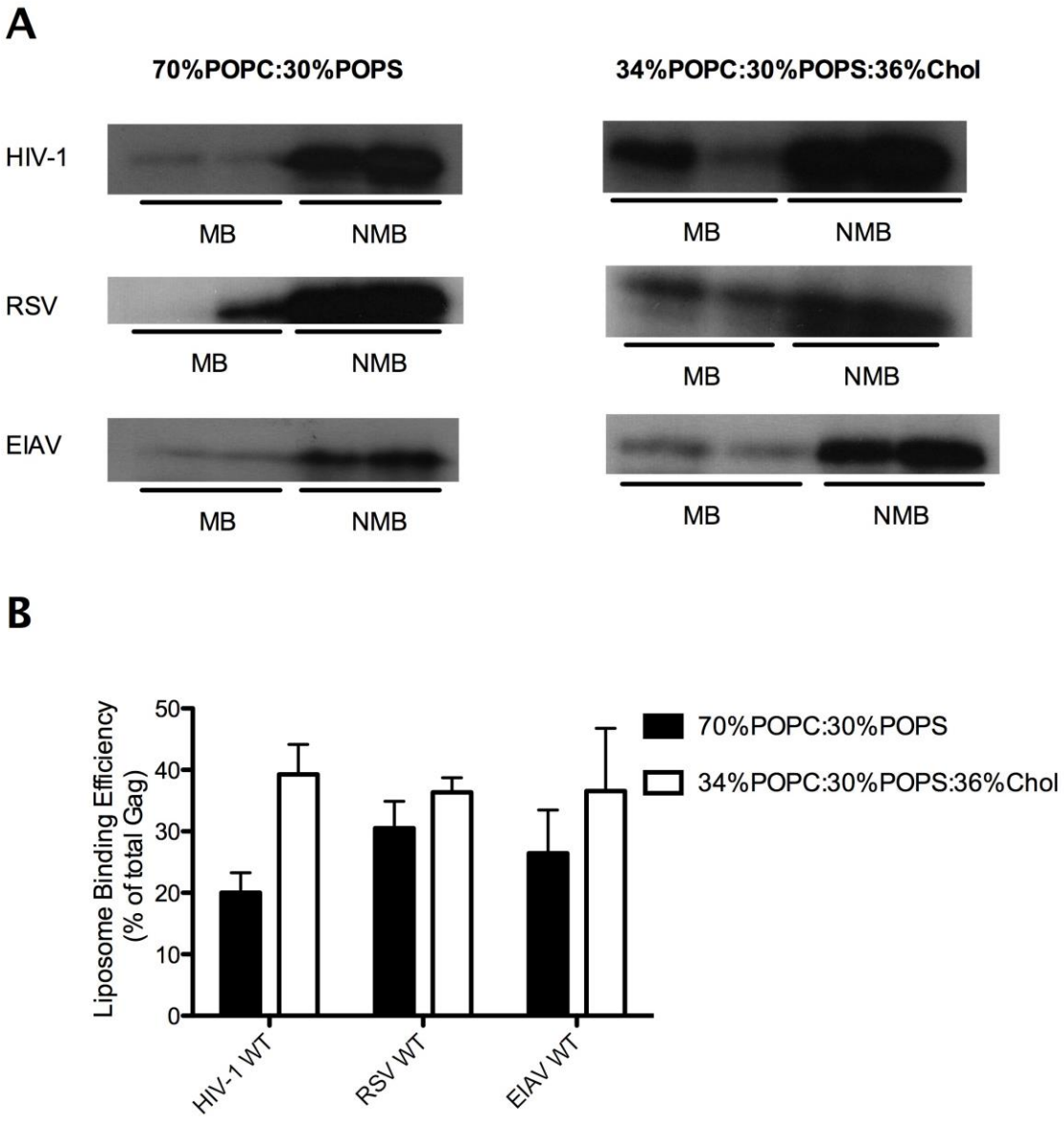
A
70%POPC:30%POPS
34%POPC:30%POPS:36%Chol
HIV-1
RSV
EIAV
MB
NMB
B
Liposome Binding Efficiency (% of total Gag)
50
40
30
20
10
0
70%POPC:30%POPS
34%POPC:30%POPS:36%Chol
HIV-1 WT
RSV WT
EIAV WT

Fig. 2

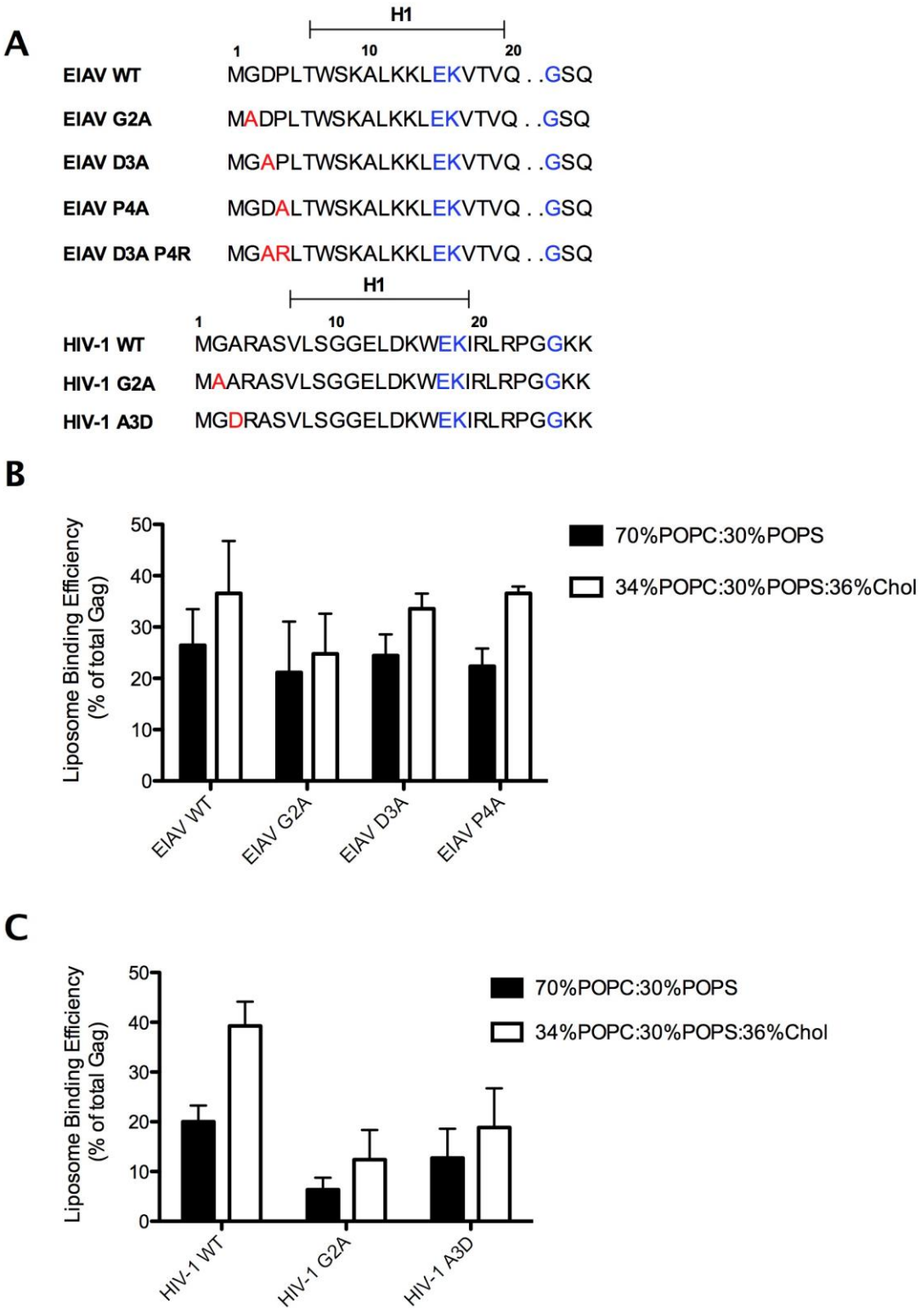
A
H1
1
10
20
EIAV WT MGDPLTWSKALKKLEKVTVQ . .GSQ
EIAV G2A MADPLTWSKALKKLEKVTVQ . .GSQ
EIAV D3A MGAPLTWSKALKKLEKVTVQ . .GSQ
EIAV P4A MGDALTWSKALKKLEKVTVQ . .GSQ
EIAV D3A P4R MGARLTWSKALKKLEKVTVQ . .GSQ
H1
1
10
20
HIV-1 WT MGARASVLSGGELDKWEKIRLRPGGKK
HIV-1 G2A MAARASVLSGGELDKWEKIRLRPGGKK
HIV-1 A3D MGDRASVLSGGELDKWEKIRLRPGGKK
B
Liposome Binding Efficiency (% of total Gag)
50
40
30
20
10
0
EIAV WT
EIAV G2A
EIAV D3A
EIAV P4A
70%POPC:30%POPS
34%POPC:30%POPS:36%Chol
C
Liposome Binding Efficiency (% of total Gag)
50
40
30
20
10
0
HIV-1 WT
HIV-1 G2A
HIV-1 A3D
70%POPC:30%POPS
34%POPC:30%POPS:36%Chol

Fig. 3

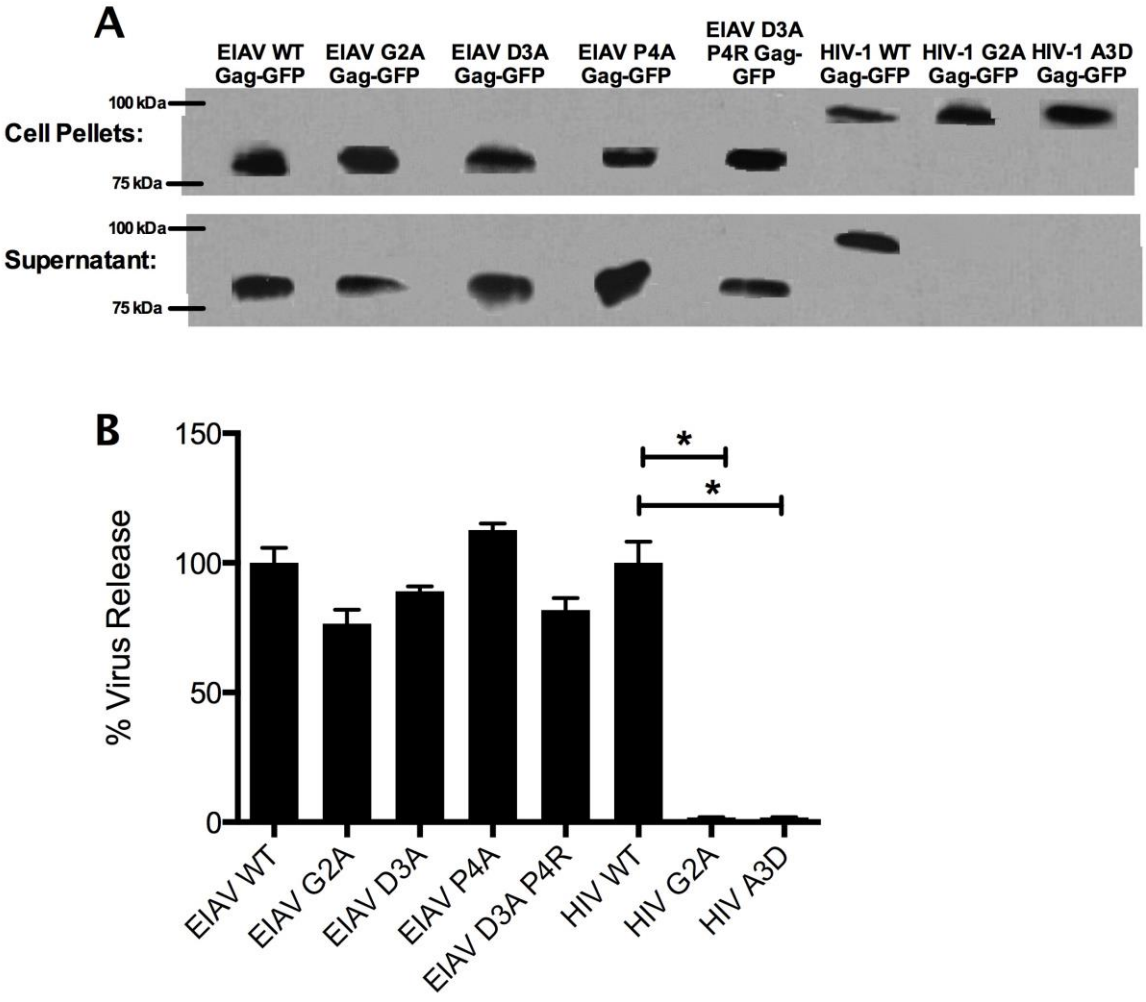
A
EIAV WT Gag-GFP
EIAV G2A Gag-GFP
EIAV D3A Gag-GFP
EIAV P4A Gag-GFP
EIAV D3A P4R Gag-GFP
HIV-1 WT Gag-GFP
HIV-1 G2A Gag-GFP
HIV-1 A3D Gag-GFP
100 kDa
Cell Pellets:
75 kDa
100 kDa
Supernatant:
75 kDa
B
% Virus Release
150
100
50
0
*
*
EIAV WT
EIAV G2A
EIAV D3A
EIAV P4A
EIAV D3A P4R
HIV WT
HIV G2A
HIV A3D

Fig. 4

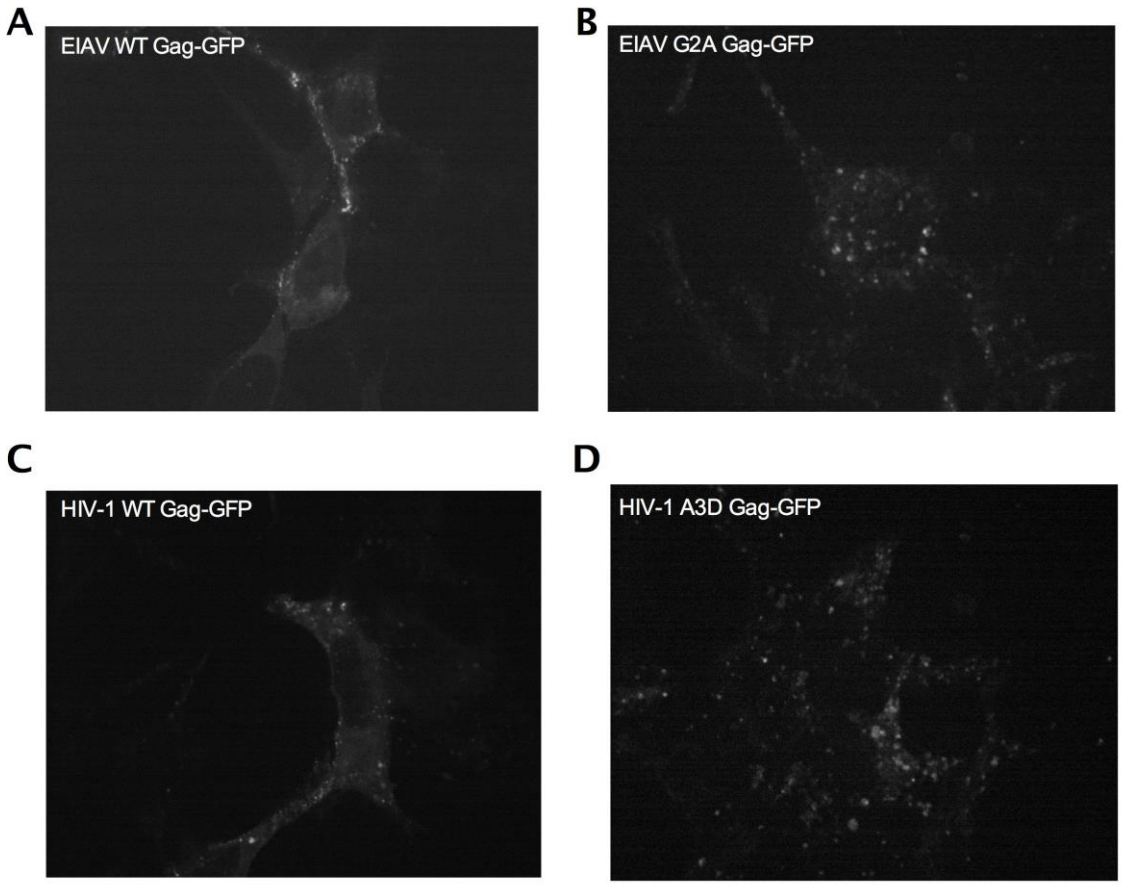
A
EIAV WT Gag-GFP
B
EIAV G2A Gag-GFP
C
HIV-1 WT Gag-GFP
D
HIV-1 A3D Gag-GFP

Appendix Fig. 1

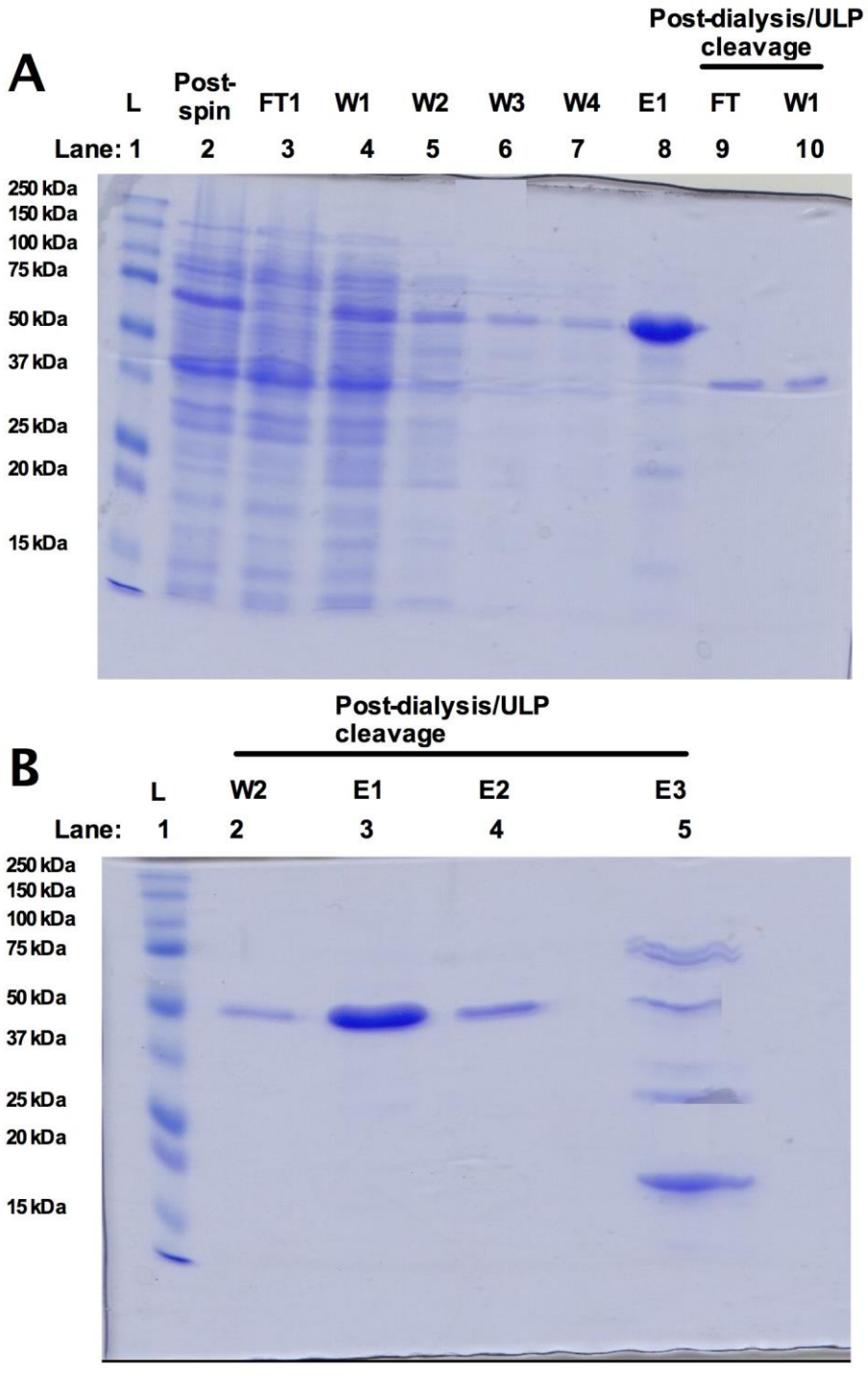

Appendix Fig. 2

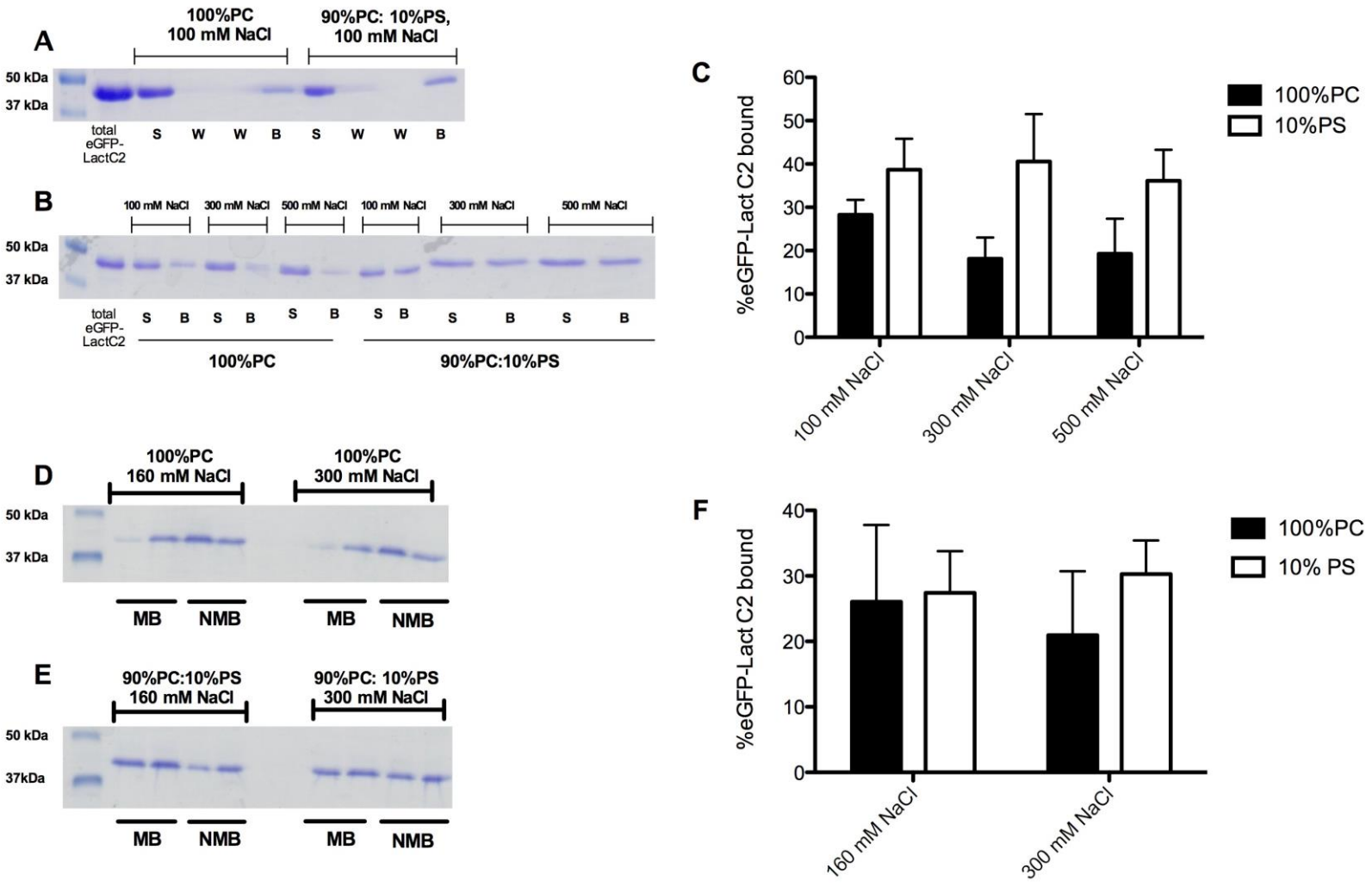

Appendix Fig. 3

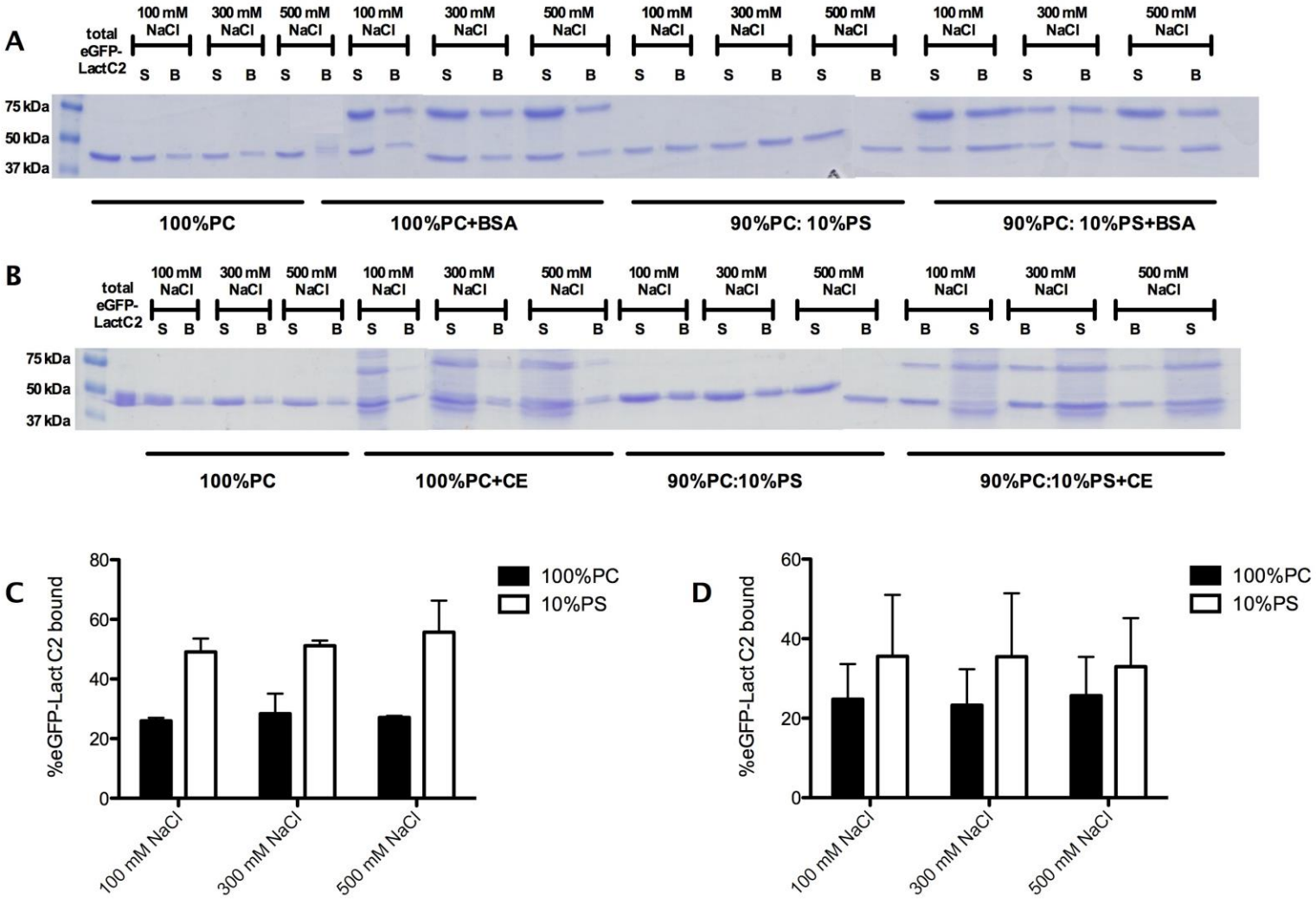

Supplementary Table 1

Construct	Cloning done by	Forward Primer	Reverse Primer
pET3xc-EIAV WT	Steven Chen	5'- CAC CAT TCT AGA ATG GGA GAC CCT TTG ACA TGG- 3'	5'- CAC CAT GAA TTC TTA CTC CCA CAA ACT GTC CAG- 3'
pET3xc-EIAV G2A	Steven Chen	5'- CAC CAT TCT AGA ATG GCA GAC CCT TTG ACA TGG AGC- 3'	5'- CAC CAT GAA TTC TTA CTC CCA CAA ACT GTC CAG- 3'
pET3xc-EIAV D3A	Steven Chen	5'- CAC CAT TCT AGA ATG GGA GCC CCT TTG ACA TGG- 3'	5'- CAC CAT GAA TTC TTA CTC CCA CAA ACT GTC CAG- 3'
pET3xc-EIAV P4A	Steven Chen	5'- CAC CAT TCT AGA ATG GGA GCC GCT TTG ACA TGG- 3'	5'- CAC CAT GAA TTC TTA CTC CCA CAA ACT GTC CAG- 3'
pET3xc-EIAV D3A P4R	Steven Chen	5'- CAC CAT TCT AGA ATG GGA GCC CGT TTG ACA TGG- 3'	5'- CAC CAT GAA TTC TTA CTC CCA CAA ACT GTC CAG- 3'
pET3xc-HIV WT	Rob Dick		
pET3xc-HIV G2A	Rob Dick		
pET3xc-HIV A3D	Steven Chen	5'- CAC CAT CAT ATG GGT GAC AGA GCG TCA GTA TTA- 3'	5'- CAC CAT GGT ACC CTA AAA ATT CCC TGG- 3'
pET3xc-RSV WT	Rob Dick		
pEGFP N1-EIAV WT	Steven Chen	5'- CAC CAT GAA TTC ATG GGA GAC CCT TTG ACA TGG- 3'	5'- CAC CAT GGA TCC AAC TCC CAC AAA CTG TCC AGG TT- 3'
pEGFP N1-EIAV G2A	Steven Chen	5'- CAC CAT GAA TTC ATG GCA GAC CCT TTG ACA TGG- 3'	5'- CAC CAT GGA TCC AAC TCC CAC AAA CTG TCC AGG TT- 3'
pEGFP N1-EIAV D3A	Steven Chen	5'- CAC CAT GAA TTC ATG GGA GCC CCT TTG ACA TGG- 3'	5'- CAC CAT GGA TCC AAC TCC CAC AAA CTG TCC AGG TT- 3'
pEGFP N1-EIAV P4A	Steven Chen	5'- CAC CAT GAA TTC ATG GGA GAC GCT TTG ACA TGG- 3'	5'- CAC CAT GGA TCC AAC TCC CAC AAA CTG TCC AGG TT- 3'
pEGFP N1-EIAV D3A P4R	Steven Chen	5'- CAC CAT GAA TTC ATG GGA GCC CGT TTG ACA TGG- 3'	5'- CAC CAT GGA TCC AAC TCC CAC AAA CTG TCC AGG TT- 3'
pEGFP N1-HIV WT	Rob Dick		
pEGFP N1-HIV G2A	Marc Johnson		

pEGFP N1-HIV A3D	Steven Chen	5'- CAC CAT GAA TTC ATG GGT GAC AGA GCG TCA GTA TTA- 3'	5'- CAC CAT GGA TCC AAA ATT CCC TGG CCT TCC CTT GTA- 3'